Petroleum Science 20 (2023) 559–568

Contents lists available at ScienceDirect

Petroleum Science

journal homepage: www.keaipublishing.com/en/journals/petroleum-science

Original Paper

Influence of carbonization temperature on cobalt-based nitrogen-doped carbon nanopolyhedra derived from ZIF-67 for nonoxidative propane dehydrogenation

Yu-Ming Li [1], Zi-Ye Liu [1], Qi-Yang Zhang, Ya-Jun Wang, Guo-Qing Cui, Zhen Zhao, Chun-Ming Xu, Gui-Yuan Jiang*

State Key Laboratory of Heavy Oil Processing, China University of Petroleum, Beijing, 102249, China

ARTICLE INFO

Article history:
Received 29 October 2021
Received in revised form
27 December 2021
Accepted 7 January 2022
Available online 20 January 2022

Edited by Xiu-Qiu Peng

Keywords:
Propane dehydrogenation
ZIF-67
Nitrogen-doped carbon
Cobalt

ABSTRACT

Propylene is a significant basic material for petrochemicals such as polypropylene, propylene oxide, etc. With abundant propane supply from shale gas, propane dehydrogenation (PDH) becomes extensively attractive as an on-purpose propylene production route in recent years. Nitrogen-doped carbon (NC) nanopolyhedra supported cobalt catalysts were synthesized in one-step of ZIF-67 pyrolysis and investigated further in PDH. XPS, TEM and N_2 adsorption-desorption were used to study the influence of carbonization temperature on as-prepared NC supported cobalt catalysts. The temperature is found to affect the cobalt phase and nitrogen species of the catalysts. And the positive correlation was established between Co^0 proportion and space time yield of propylene, indicating that the modulation of carbonization temperature could be important for catalytic performance.

1. Introduction

Propylene is the useful raw material for the production of a number of important chemicals and polymers including polypropylene, acrylonitrile, propylene oxide and other industrial products. Conventional propylene production routes involve fluid catalytic cracking and steam cracking of naphtha. However, these routes cannot meet the increasing future demand for propylene, due to the rapid development of social society. Therefore, the developing of highly efficient propylene production technologies is of importance in both science and economy (Lavrenov et al., 2015). Nonoxidative propane dehydrogenation (PDH) calls much attention recently, as an on-purpose propylene production route, for its high propylene selectivity and abundant propane supply from shale gas. Significant research has focused on Pt and Cr-based catalysts as well as alloys of these metals and other metal oxides (Motagamwala et al., 2021). The industrial Pt and Cr-based catalysts, being commercialized catalysts with high efficiency, are obstructed by high cost and environmental/health concerns. Therefore, a strong motivation exists to discover or investigate earth-abundant elements with environmental harmless to replace Pt and Cr based catalysts (Hu et al., 2019). The abundance of Co on earth can ensure its long-term application prospect, and the cobalt-based catalysts recently were reported by several groups which showed good performance in C–H bond activation for alkane molecules (Dai et al., 2020; Ma and Ackermann, 2015; Zhao et al., 2019b).

Metallic Co^0, isolated and aggregated Co^{2+} or/and Co^{3+} are deemed as the active sites for C–H activation (Estes et al., 2016; Hu et al., 2015; Li et al., 2018). Although Co-based catalysts attract appreciable attention in PDH, the activity still needs to be improved. Additive modification and support variation are known to be efficient routes (Chen et al., 2020; Dai et al. 2020; Dewangan et al., 2019; Li et al. 2018; Sun et al., 2015; Zhao et al., 2018). Zr, S and Ni were reported to improve the dispersion of Co species and metal-support interaction which could further enhance the activity in PDH (Sun et al. 2015; Wang et al., 2018, Zhao et al., 2018). Besides, the support has been regarded as a key point to influence the catalytic performance which could tune the structure of cobalt species (Blanch-Raga et al., 2016; Held et al., 2018; Otroshchenko et al., 2016).

* Corresponding author.
E-mail address: jianggy@cup.edu.cn (G.-Y. Jiang).
[1] These authors contributed equally.

https://doi.org/10.1016/j.petsci.2022.01.008

Recently, nitrogen-doped carbon (NC) supported nonprecious metals-based catalysts were developed for the electrocatalysis with comparable activity and stability to the well-known Pt catalysts (Zhang et al., 2014). On the basis of this, NC supported metal catalysts were further introduced into C–H activation reactions such as F-T synthesis (Lu et al., 2014) and propane dehydrogenation (Wang et al., 2021; Ye et al., 2019; Zhao et al., 2019a). Especially for NC introduction, not only could the stability of metal species be enhanced, but also the electronic structure of active sites could be modified (Dlamini et al., 2020; Wang et al., 2021). Moreover, NC species in the catalyst could form stable nitrogen-metal bond, and this could modulate the electronic environment, chemical valence and stability of metal species. This can further improve the catalytic performance through enhancement of reactant activation. Meanwhile, metal-organic frameworks (MOFs) constructed by periodically arranged organometallic ligands and metal ions with 3D structure have been used as hard templates for preparing NC supported metal catalysts. With this strategy, catalysts with high metal content and high dispersion of the metallic nanoparticles could be prepared. And owing to their high specific surface area, chemical tunability and well metal-support interaction, NC supported metal catalysts show excellent catalytic performance including C–H bond activation of alkanes (Cao et al., 2017).

ZIF-67 is a well-known metal-organic framework which is composed of Co^{2+} coordinating metal clusters and 2-methylimidazole organic ligands. And NC supported cobalt-based catalysts derived from ZIF-67 are attractive alternatives to noble metal-based catalysts. With carbonization under inert atmosphere, ZIF-67 could act as self-sacrificing template to provide carbon, nitrogen and cobalt sources simultaneously. Cobalt species homogeneously distributed throughout the carbon matrix in the hybrid could be achieved, which is also reported to possess good resistance to extensive agglomeration and sintering even at high temperature. In PDH study, some excellent works with NC materials have been reported (Cao et al., 2021; Wang et al. 2021). However, the field is still at an early stage, and the research of ZIF-67 derived NC supported cobalt catalysts still needs deep investigation in PDH.

The work herein demonstrates the evolution of ZIF-67 derived cobalt catalysts with the increase of carbonization temperature, and studies their unique catalytic performance in PDH. NC support and Co active sites were formed simultaneously during carbonization of ZIF-67. TEM, XPS and N_2 adsorption-desorption were used to reveal the relationship between carbonization temperature and existing states of nitrogen species and Co species. The so-prepared catalysts were investigated in PDH reaction at 550 °C. Owing to the modulation of nitrogen species and cobalt species, the catalytic performance showed high correlation of Co^0 with space time yield of propylene.

2. Experimental

2.1. Catalyst preparation

All chemicals used in this work were of analytical grade and used as received. $Co(NO_3)_2{\cdot}6H_2O$ and 2-methylimidazole were brought from Shanghai Aladdin Biochemical Technology Co., Ltd. CH_3OH was obtained from Tianjin Jingdongtianzheng Precision Chemical Reagent Factory.

ZIF-67 was prepared by the method reported in literature (Zhang et al., 2019). In brief, $Co(NO_3)_2{\cdot}6H_2O$ was firstly dissolved in methanol followed by 2-methylimidazole addition. After stirring at room temperature for 24 h, the mixture was aged for another 12 h. The precipitate could be obtained by centrifugation, washing and drying at 80 °C overnight. NC supported cobalt catalyst was prepared after carbonization of as-synthesized precipitate at different temperatures in the range of 550–900 °C under N_2 atmosphere. The obtained sample was named as Co/NC-T, where T stands for carbonization temperature.

2.2. Characterizations

XRD (Bruker D8 Advance) was used to determine the phase structure of as-prepared samples with CuKα radiation operated at 40 kV and 30 mA. Micro-morphology and cobalt particle size of as-prepared samples were analyzed by scanning electron microscopy (SEM, FEI-Quanta 250 FEG) and transmission electron microscopy (TEM, Philips FEI Tecnai G2 F20).

The texture property of Co/NC-T was obtained from N_2 adsorption-desorption isotherm which was recorded by ASAP 2460 Micromeritics at −196 °C. A certain amount of as-prepared sample was pretreated in vacuum at 90 °C for 1 h and 350 °C for 3 h before test. Brunauer-Emmett-Teller (BET) equation and t-plot method were used for data analysis. ICP-OES for Co loading analysis was carried on by Agilent ICPOES730. XP spectra were recorded on Thermo ESCALAB 250Xi, and C 1s at 284.6 eV was used for calibration. And all XP spectra were subtracted with their background spectra.

2.3. Propane dehydrogenation

Propane dehydrogenation was carried on in a micro fixed-bed reactor. In a typical run, 50 mg of as-prepared sample was pressed into 40–60 mesh and filled into a quartz reactor with 6 mm diameter. The temperature was elevated to 550 °C in N_2, and 40% C_3H_8/N_2 with total flow rate of 10 mL/min was introduced. After 10 min stabilization process, PDH reaction was then started. All the products including propylene, ethylene, ethane and methane during the reaction were analyzed with an on-line gas chromatography (TP-3420 from Beijing Beifen-Ruili analytical instrument Co., Ltd.), which was equipped with a FID detector and a capillary column of Agilent 115–3532.

Conversion of propane, selectivity to propylene, space time yield of propylene and deactivation coefficient (k_d) are calculated by equations (1)-(4), respectively.

$$X(C_3H_8) = \frac{F(C_3H_8,in) - F(C_3H_8,out)}{F(C_3H_8,in)} \times 100\% \quad (1)$$

$$S(C_3H_6) = \frac{F(C_3H_6,out)}{F(C_3H_8,in) - F(C_3H_8,out)} \times 100\% \quad (2)$$

$$STY(C_3H_6) = \frac{F(C_3H_8,in) \times S(C_3H_6) \times X(C_3H_8) \times M(C_3H_6)}{V_m \times m_{cat}} \quad (3)$$

$$k_d = \frac{ln\left(\frac{1-X_{end}}{X_{end}}\right) - ln\left(\frac{1-X_{start}}{X_{start}}\right)}{t} \quad (4)$$

In the equations, $X(C_3H_8)$, $S(C_3H_6)$ and $STY(C_3H_6)$ represent propane conversion, propylene selectivity and space time yield of propylene, respectively. $F(C_xH_y,in)$ and $F(C_xH_y,out)$ are named for mole ratio of inlet and outlet C_xH_y. $M(C_3H_6)$, V_m and m_{cat} are abbreviated for propylene mole weight, standard molar volume of gas and catalyst weight, respectively. For deactivation coefficient (k_d), equation (4) is used. In the equation, X_{end} and X_{start} denote propane conversion at the beginning and at the end of the long stability test, respectively, and t is abbreviated for duration time of the stability test.

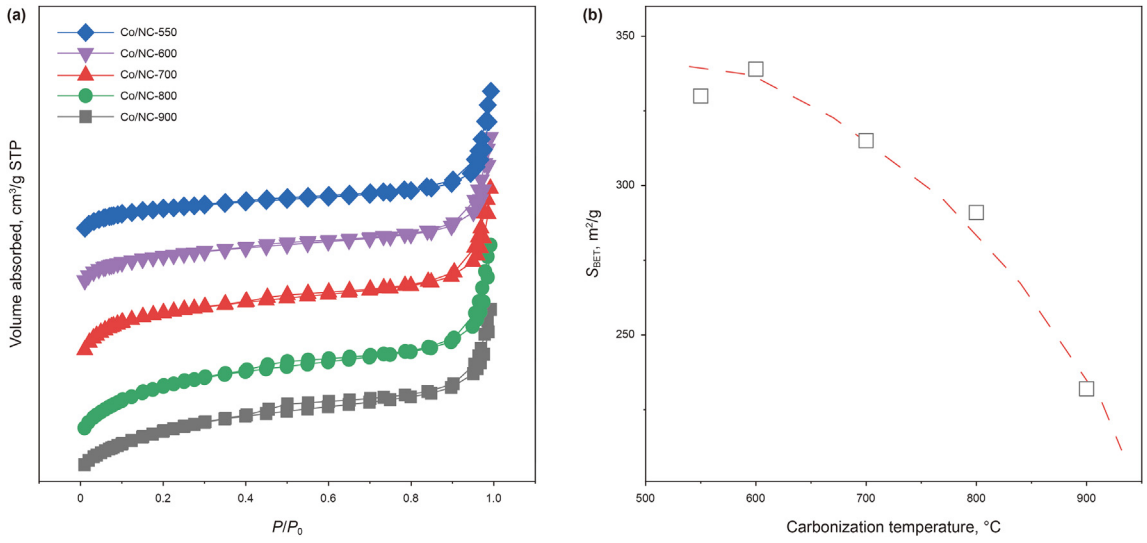

Fig. 1. (a) Nitrogen adsorption-desorption isotherms of as-prepared Co/NC-T and (b) influence of carbonization temperature on BET specific surface area.

Table 1
Texture properties of as-prepared Co/NC-T.

Sample	Specific surface area[a], m^2/g	Micropore volume[b], cm^3/g	Total volume[c], cm^3/g	Co content[d], wt%
Co/NC-550	328	0.12	0.16	30.2
Co/NC-600	339	0.12	0.16	31.6
Co/NC-700	315	0.08	0.18	36.3
Co/NC-800	291	0.04	0.22	41.3
Co/NC-900	232	0.02	0.19	38.9

Note.
[a] Specific surface area calculated by BET equation.
[b] Micropore volume calculated by t-plot method.
[c] Total pore volume calculated by BJH absorption.
[d] Contents of Co were determined by ICP-OES.

3. Results and discussion

3.1. Texture property, phase structure and micromorphology

N_2 adsorption-desorption isotherms, pore size distributions and other texture properties are shown in Fig. 1, Fig. S1 and Table 1. From Fig. 1a, all the samples exhibit steep increases of typical type I isotherms at very low relative pressure, indicating the presence of micropores. With t-plot method and BET equation, texture properties of as-prepared Co/NC-T are listed in Table 1. It should be noticed that the carbonization temperature largely influences texture property of as-prepared samples, especially for the specific surface area. From Fig. 1b, with increasing carbonization temperature from 550 °C to 900 °C, the specific surface area decreased rapidly from ~330 to 232 m^2/g, indicating the strong impact of carbonization temperature on the structure of ZIF-67. Moreover, it should be noted that present catalysts are incorporated by cobalt species with mass content around 30–42 wt%.

To elucidate the effect of carbonization temperature on morphology and phase structure of the resulting Co/NC-T samples, SEM and XRD characterizations were conducted, and the results are shown in Fig. 2 and Fig. S2. It can be found in Fig. S2 that the geometric shape of ZIF-67 crystal is regular rhombic dodecahedral morphology composed of well-defined rhombus faces and straight edges which is in accordance with the literature (Wang et al., 2019). Normally, with high temperature carbonization, the shape would gradually shrink, especially with high temperature and long carbonization time. Thus, for the samples carbonized at different temperatures, with elevating the carbonization temperature, the morphology of as-prepared catalysts evolved step by step from a smooth morphology to nanometer-sized non-ordered carbon.

From Fig. 2, it is clear that after direct carbonization at lower than 700 °C, ZIF-67 converted into nitrogen-doped carbon with retaining its original micromorphology. The overall particle size and shape of NC nanopolyhedra were similar to that of ZIF-67, while the surface of NC appeared distortion and bumpiness after carbonization. The high carbonization temperature at higher than 800 °C made ZIF-67 transform into non-regular carbon materials with distorted small particles on the surface, indicating that high temperature would destroy the MOFs morphology in a large scale.

Phase structure of as-prepared samples at varying carbonization temperatures were analyzed by XRD patterns shown in Fig. 2f. All the samples underwent structural transformation after carbonization, which are in accordance with SEM images. There are mainly two characteristic peaks at 44.2° and 51.6°, respectively, which can be clearly observed for all Co/NC-T samples, corresponding to face-centered-cubic (fcc) Co crystals of (111) and (200) diffractions. Meanwhile, with carbonization temperature gradually increased from 550 °C to 800 °C, the intensity and sharpness of the peaks corresponding to (111) and (200) of fcc Co crystals increases rapidly. At 900 °C of carbonization, the phase structure changed dramatically. Although the characteristic peaks of fcc Co crystal can still be observed, the diffraction peak at around 25°, representing (002) interlayer of carbon, becomes more obvious. And such carbon might be the stacking structure of aromatic layers (Yoshizawa et al., 2000). This implies the formation of carbon with a higher

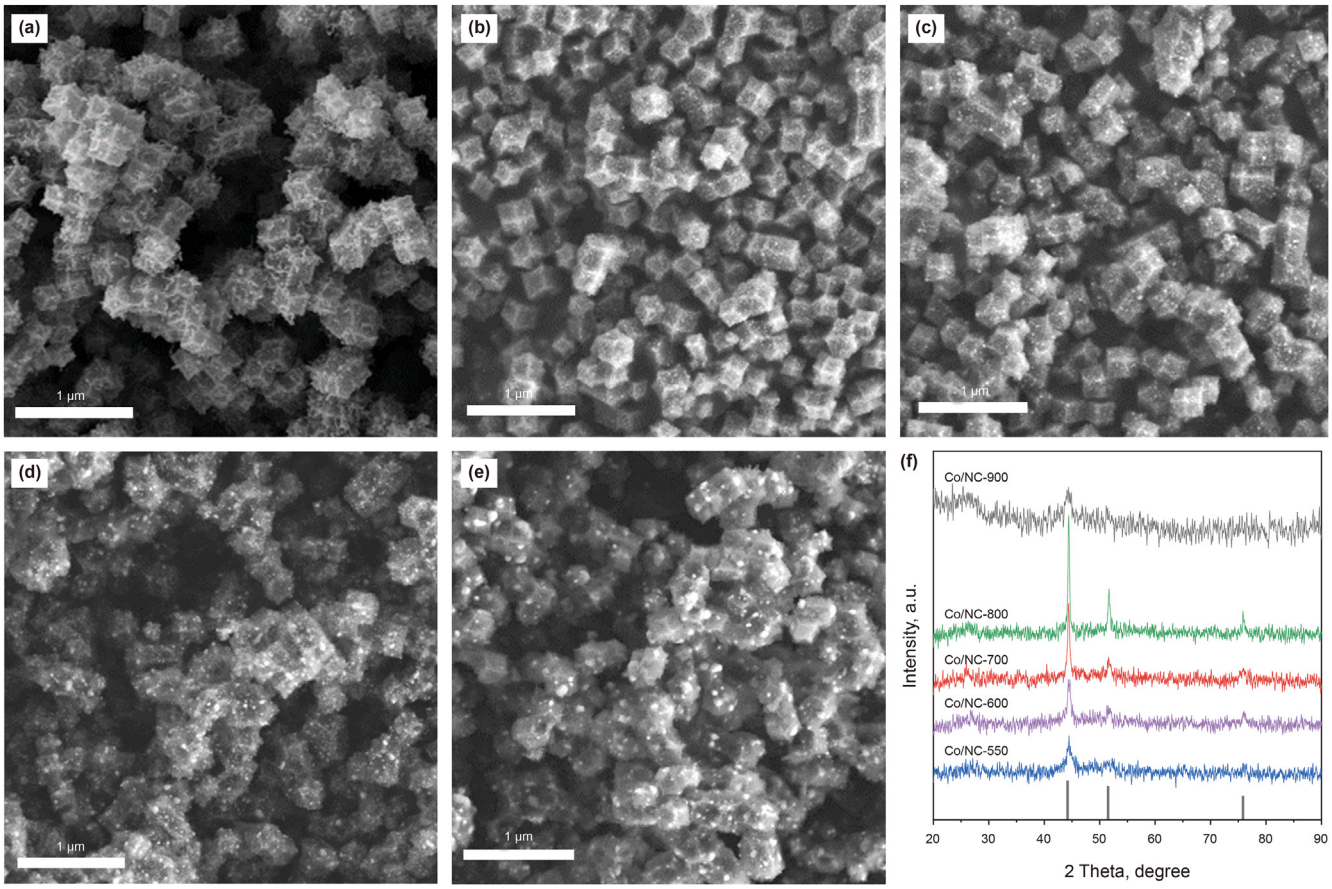

Fig. 2. SEM images of (a) Co/NC-550, (b) Co/NC-600, (c) Co/NC-700, (d) Co/NC-800, (e) Co/NC-900, and (f) XRD patterns of as-prepared Co/NC-T.

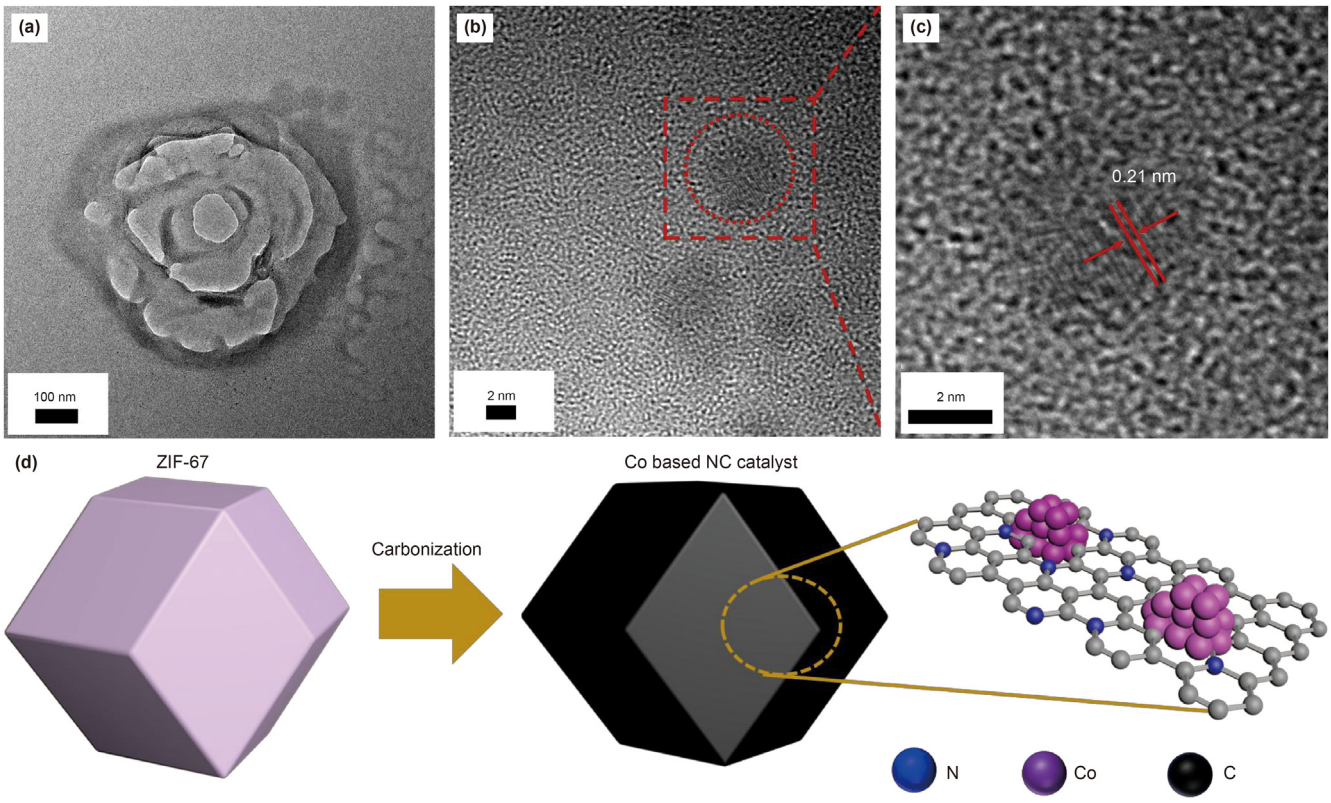

Fig. 3. TEM images of Co/NC-700 (a–c) and synthesis process scheme (d).

graphitization degree and the destroy of MOFs structure which was also reported by other literature (Guo et al., 2017).

3.2. Distribution and nature of Co species

As mentioned above, the carbonization of ZIF-67 would result in rearrangement of the constituent atoms and collapse of microporous structure, forming cobalt species located on NC support. TEM images were recorded to provide more details about the structure and cobalt distribution of as-prepared sample, and the results are shown in Fig. 3a–c with EDX mapping images in Fig. S3. EDX images confirmed that after carbonization, Co/NC-700 contains homogenously dispersed N and Co species. From TEM image in Fig. 3b, it is noted that cobalt nanoparticles are distributed on the NC surface. Crystal structure of Co nanoparticles could be further illustrated in Fig. 3c. The lattice fringe of 0.21 nm can be found, which is perfectly matched with (111) interplanar distance of fcc Co. And this is also in accordance with XRD patterns in Fig. 2. On this basis, the schematic illustration of preparation process for Co/NC-T could be drawn in Fig. 3d.

UV–Vis spectra of as-prepared samples were recorded to analyze the dispersion of Co nanoparticles which are shown in Fig. S4. Only one broad peak at around 300–400 nm could be observed which belongs to electron transfer from O to Co species. The nature and coordination of the cobalt, carbon and nitrogen species of as-prepared catalysts were examined by XPS, which are shown in Fig. 4 and Figs. S5–S7. Co/NC-700 was taken as the example to analyze in detail. The XPS survey spectrum (Fig. 4a) of Co/NC-700 shows signals of C, N, O and Co elements which suggests that Co and N species have been introduced into as-prepared sample.

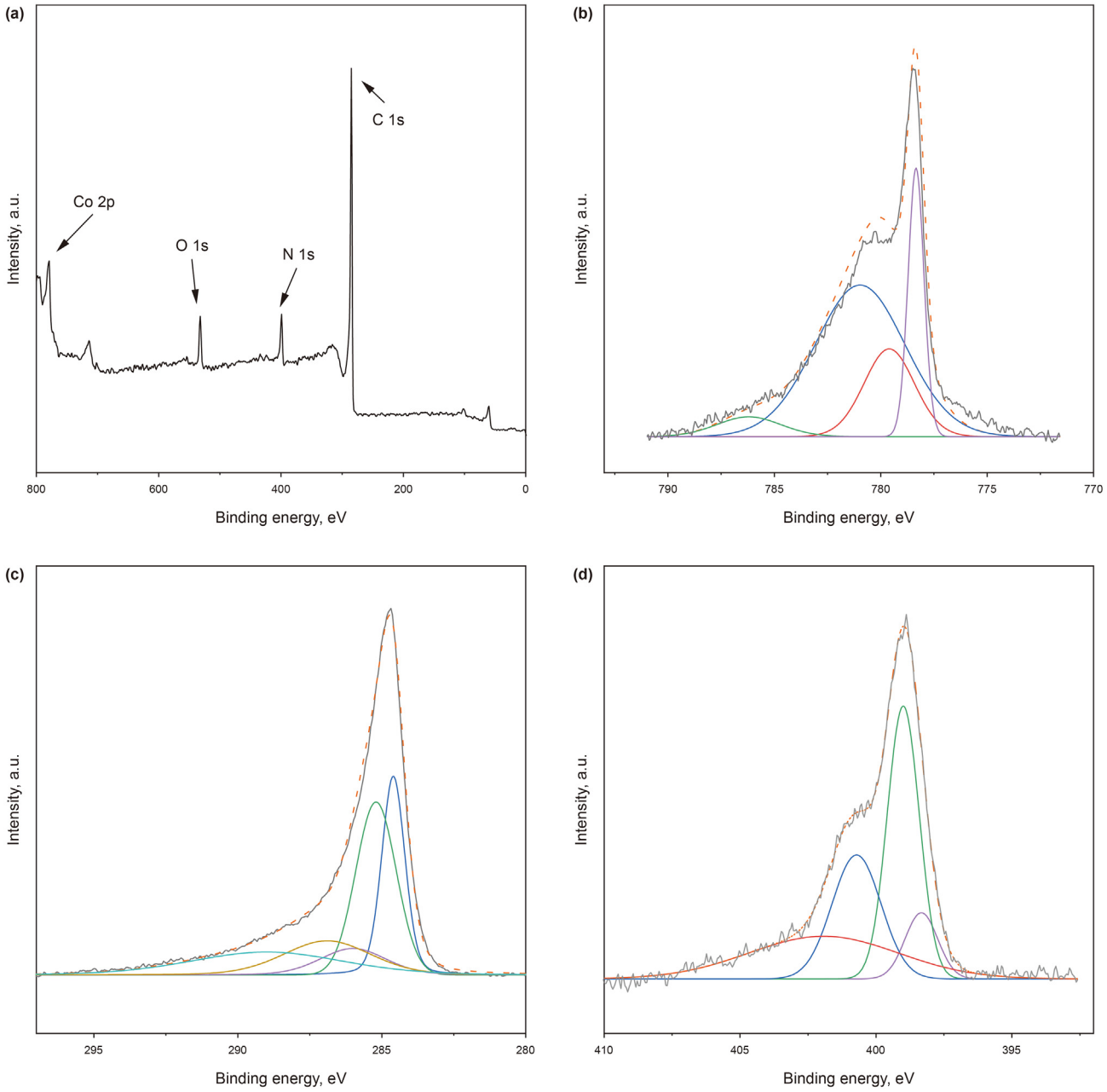

Fig. 4. XPS survey spectrum (a), Co 2p XP spectrum (b), C 1s XPS spectrum (c) and N 1s XPS spectrum (d) of Co/NC-700.

Co $2p_{3/2}$ XPS spectrum of Co/NC-T in Fig. 4b and Fig. S5 exhibited the major peaks at around 778 and 781 eV, indicating the presence of Co^0 and N–Co species. According to the references (Gao et al., 2019; Zhang et al., 2015), after deconvoluting of Co $2p_{3/2}$ XP spectrum, another two peaks could be found locating at around 780 and 786 eV, which represent Co^{2+} and satellite of Co^{2+} and/or Co^0. This indicates that Co species in ZIF-67 could transform into Co with valence of 0 and + 2, and coordinate well with the existed nitrogen species.

During the carbonization process, ligands (2-methylimidazole) would form substantial carbon-based moieties on the surface of the carbon materials. To probe these groups, C 1s XP spectra were collected and shown in Fig. 4c and Fig. S6, and five peaks could be deconvoluted. The two main peaks locating at 284.6 and 285.2 eV, assigning to sp^2-hybridized graphite-like carbon and sp^3-hybridized diamond-like carbon, respectively, could be observed. Besides, the other three peaks centered at around 286.0, 286.9 and 289.0 eV could be attributed to C–O, C–N and C═O/C═N, respectively (Han et al., 2016).

As shown in Fig. 4d and Fig. S7, the high resolution N 1s spectrum can be deconvoluted to four sub-peaks due to the spin-orbit coupling. Pyridinic N (398.5 eV), N in N–Co species (399.0 eV), pyrrolic N (400.2 eV) and graphitic N (402.1 eV) could be assigned (Gao et al., 2019). The N–Co bond is formed by bonding N atoms with Co atoms, which is also reported by other literature (Zhan et al., 2017). This N–Co species can also be observed in Co 2p XP spectra. By combination of C 1s spectrum, the presence of N–Co and C–N/C═N species in as-prepared samples suggests the

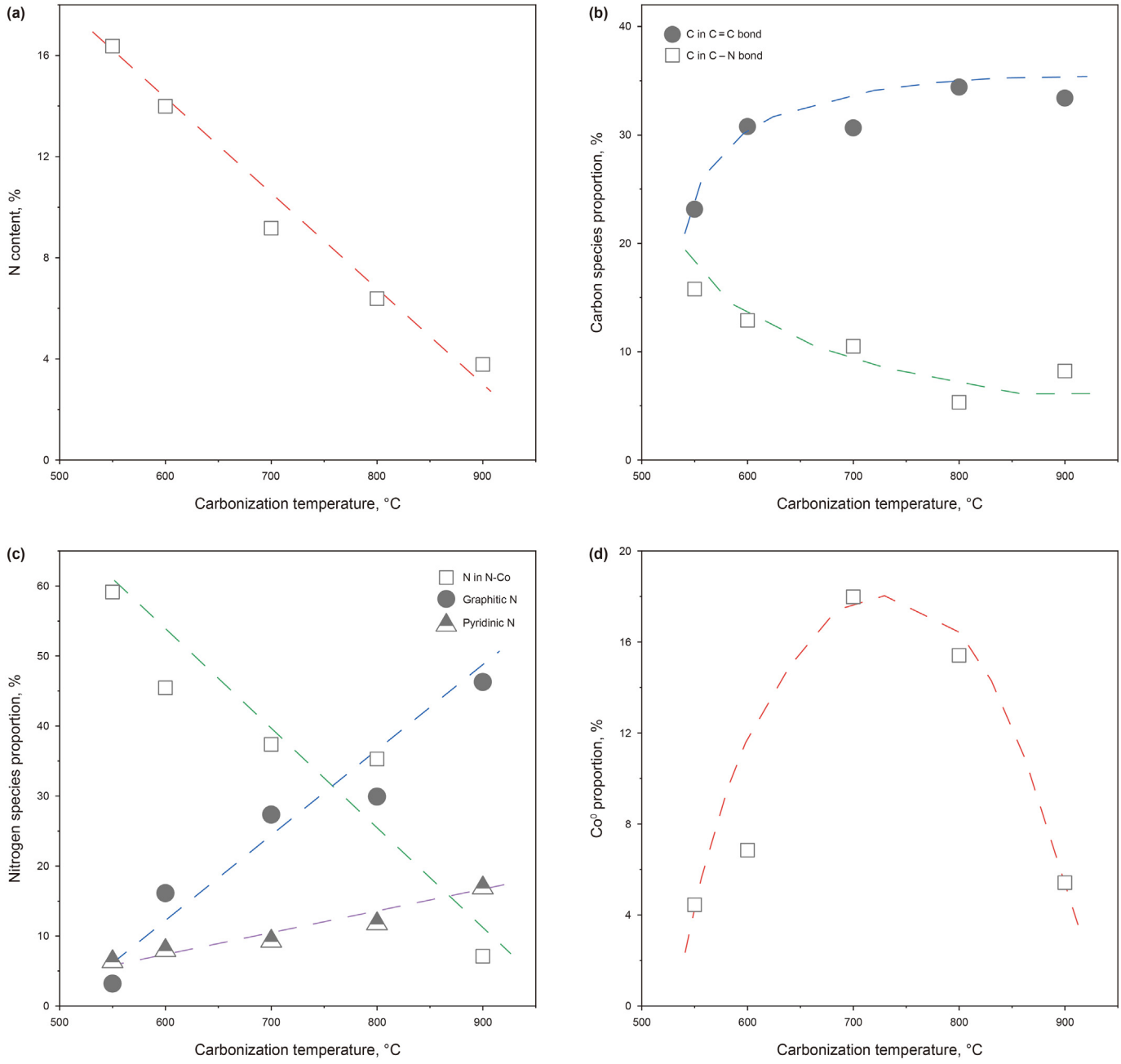

Fig. 5. Function of carbonization temperature on (a) N content, (b) C species distribution, (c) N species distribution and (d) Co^0 proportion.

successful formation of Co–N–C, which is attributed to the transformation of C–C bonds at the interface between Co NPs and nitrogen-doped carbon.

Meanwhile, the corresponding element contents analyzed by XPS are listed in Table S1, and the function of carbonization temperature on element content is shown in Fig. 5. With carbonization temperature increased from 550 °C to 900 °C, N content on Co/NC-T would directly decrease from 16.4% to 3.8% (Fig. 5a). This illustrates that the MOFs-driven synthesis method can easily control the nitrogen-doped concentration by varying the carbonization temperature. Accompanied by N content decreasing, proportion of C–N bond related carbon species was found to be decreased from 15.8% to around 8%, while the proportion of C in C=C bond increased from 23.1% to around 34% (Fig. 5b), indicating the thermally unstable nature of nitrogen species in the framework. As shown in Fig. 5c, with elevating carbonization temperature, the relative content of graphitic N species progressively increased from 3.2% to 46.3%, while N–Co species dramatically decreased from 59.1% to 7.1%. These results are in accordance with C 1s spectra, suggesting the instability of N–Co bond and its easy conversion to graphitic N species at high temperatures. It is worth noticing that the proportions of Co species in different chemical valences were modulated by carbonization temperature, especially for Co^0 (Fig. 5d). At 550 °C, the proportion of Co^0 is 4.4%, and with increasing carbonization temperature, Co^0 proportion reached the maximum of 18.0% at 700 °C. Further elevating carbonization temperature to 900 °C, Co^0 proportion decreased to only 5.4%.

It is known that nitrogen and carbon species in NC material may

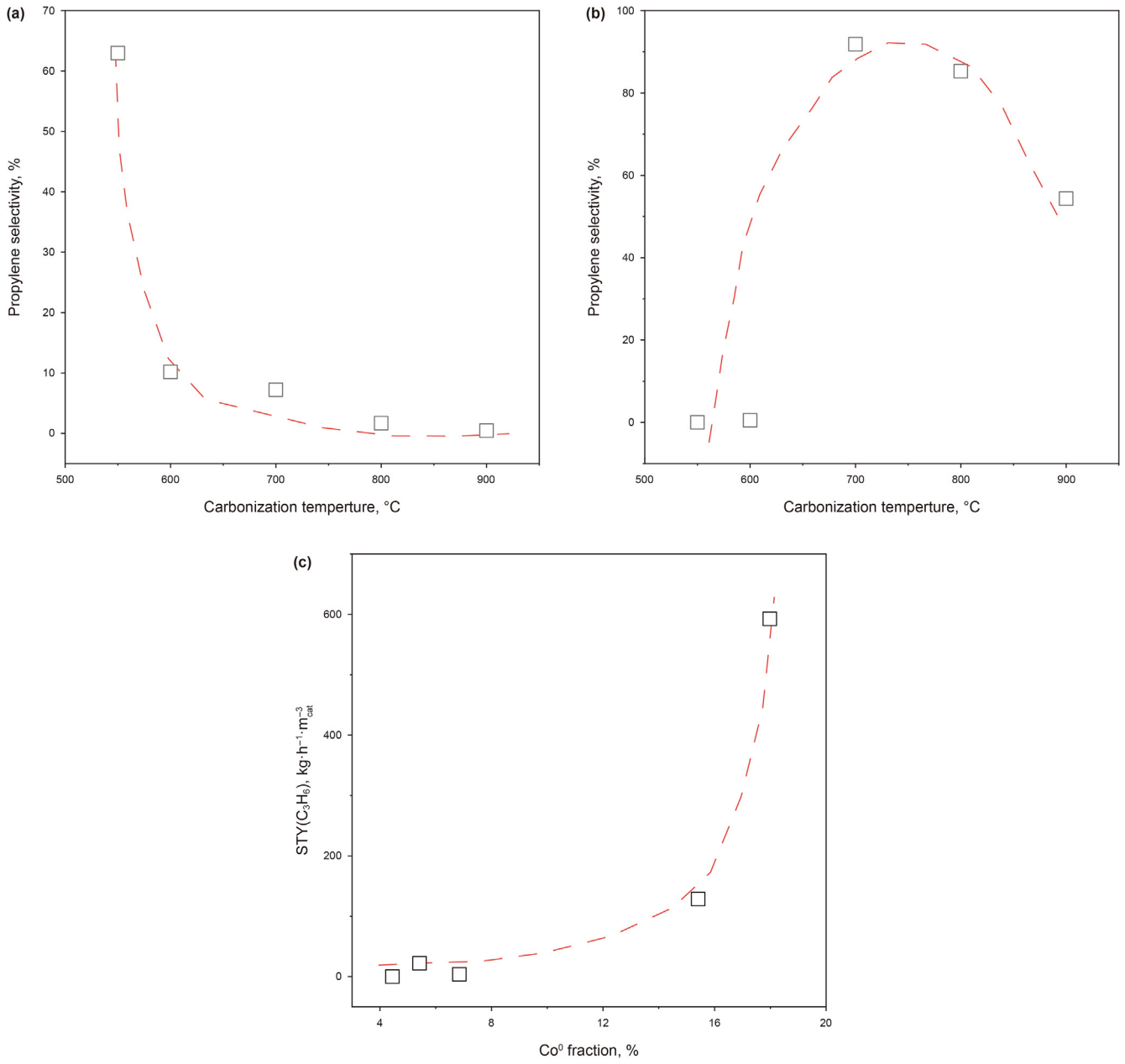

Fig. 6. Influence of carbonization temperature on catalytic performance of as-prepared Co/NC-T (a) initial propane conversion, (b) initial propylene selectivity, and (c) influence of Co^0 proportion on STY(C_3H_6).

influence metal species, especially the chemical valence and coordination environment. It might be concluded here that at low carbonization temperature, the enrichment of N–Co species could prevent the formation of metallic Co^0. With elevating temperature, these N–Co species would gradually decompose and transform to Co^0. Meanwhile, the surface nitrogen species, especially pyridinic N and graphitic N, which could also interact with metal species, could be formed at high carbonization temperature. And thereafter, these pyridinic N and graphitic N would hinder the formation of Co^0. The coordination of these two opposite factors makes Co^0 proportion reach its maximum at 700 °C.

3.3. Propane dehydrogenation over Co/NC-T

As-prepared Co/NC-T catalysts were introduced into PDH, and the influence of carbonization temperature on catalytic performance is shown in Fig. 6 and Fig. S7. With carbonization at 550 °C, Co/NC-550 possesses the highest propane conversion of 63.0%, but no propylene could be found. All propane molecules were converted into by-products including methane, ethane, ethylene and coke. It is clearly shown that the initial propane conversion decreased largely from 63.0% to 10.2% with carbonization temperature elevating to 600 °C, and very rare propylene could be observed. When carbonization temperature was increased to 700 °C, propylene could be obviously formed. For Co/NC-700, it possessed the highest propylene selectivity of 91.9%, with propane conversion of 7.2%. Continually increased temperature to 900 °C, propylene selectivity then decreased to 54.3%.

The difference in product distribution might be caused by the variation of Co species on Co/NC-T, which could be modulated by

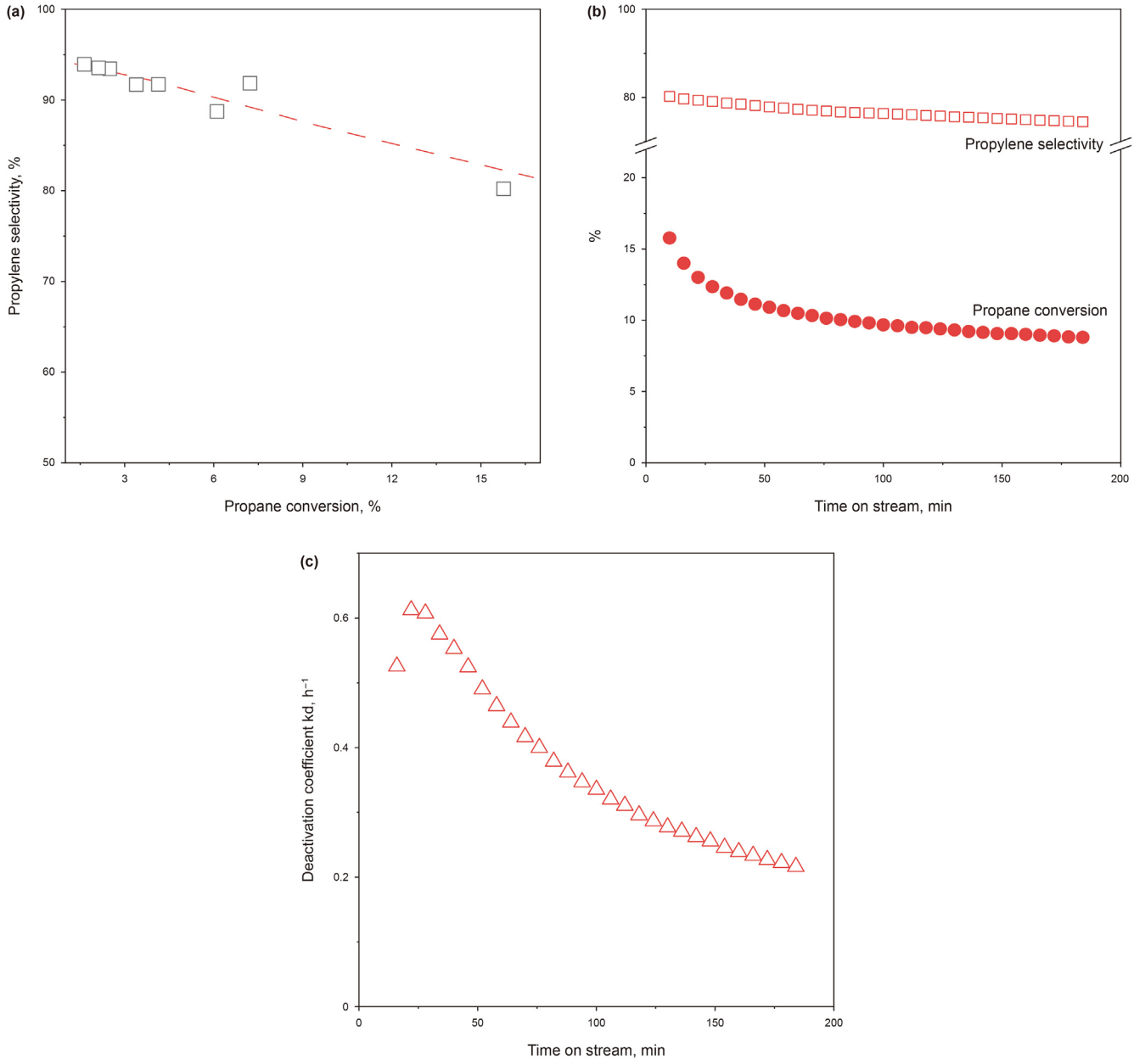

Fig. 7. Conversion-selectivity relationship (a), time-on-stream stability test (b) and deactivation coefficient k_d during reaction (c) over as-prepared Co/NC-700.

carbonization temperature. It should be noticed that STY(C_3H_6) value has positive relationship with metallic Co^0 proportion, as illustrated in Fig. 6c. With Co^0 proportion increased from 4.4% to 18.0%, the STY(C_3H_6) was improved from 0 to 592.5 kg $h^{-1}\cdot m^{-3}_{cat}$. In combination with XPS spectra analysis, it could be deduced here that the control of carbonization temperature could modulate Co^0 proportion on the surface of Co/NC-T through nitrogen and carbon species variation. The highest proportion of Co^0 at 700 °C carbonization would also lead to the highest space time yield of propylene (STY(C_3H_6)), indicating the importance of metallic Co^0 on propane to propylene.

To further investigate the catalytic performance of Co/NC-700, propane conversion-propylene selectivity relationship was established by varying propane conversion, which is shown in Fig. 7a. Accompanied by the increase of propane conversion from 1.6% to 15.8%, propylene selectivity decreased from 94.0% to 80.2%. This might be caused by the transformation of propylene to by-products at a high level of propane conversion. Time-on-stream stability test of 180 min was also carried on and the result is shown in Fig. 7b. During the process, propane conversion decreased fast at the beginning 50 min, from 15.8% to 11.1%. For the next 130 min, propane conversion slowly decreased from 11.1% to 8.8%. This could also be drawn by deactivation coefficient k_d variation, which showed directly decrease from around 0.6 h^{-1} to 0.22 h^{-1} (Fig. 7c). During stability test, propylene selectivity showed a slightly decrease from 80.2% to 74.5%.

4. Conclusion

A series of NC nanopolyhedra supported cobalt catalysts were synthesized with a one-step ZIF-67 pyrolysis strategy by modulating carbonization temperature. With the increase of carbonization temperature, the proportion of nitrogen species, such as N–Co, pyridinic N and graphitic N, were variated which would tune the composition of cobalt species. So designed catalysts demonstrate positive correlation between Co^0 proportion and STY(C_3H_6), indicating the significance of Co^0 species for propylene formation. This efficient modulation of MOFs-derived non-noble metal-based catalysts may provide new insights into the design of highly effective catalysts in PDH.

Acknowledgement

This work is supported by the National Natural Science Foundation of China (Grant Nos. 21802167, 21961132026, 92034302, 21878331, 91645108), the National Key Research and Development Program Nanotechnology Specific Project (No. 2020YFA0210903).

Appendix A. Supplementary data

Supplementary data to this article can be found online at https://doi.org/10.1016/j.petsci.2022.01.008.

References

Blanch-Raga, N., Palomares, A.E., Martínez-Triguero, J., et al., 2016. Cu and Co modified beta zeolite catalysts for the trichloroethylene oxidation. Appl. Catal. B Environ. 187, 90–97. https://doi.org/10.1016/j.apcatb.2016.01.029.

Cao, T., Dai, X., Li, F., et al., 2021. Efficient non-precious metal catalyst for propane dehydrogenation: atomically dispersed cobalt-nitrogen compounds on carbon nanotubes. ChemCatChem 13 (13), 3067–3073. https://doi.org/10.1002/cctc.202100410.

Cao, Y., Mao, S., Li, M., et al., 2017. Metal/Porous carbon composites for heterogeneous catalysis: old catalysts with improved performance promoted by N-doping. ACS Catal. 7 (12), 8090–8112. https://doi.org/10.1021/acscatal.7b02335.

Chen, C., Zhang, S., Wang, Z., et al., 2020. Ultrasmall Co confined in the silanols of dealuminated beta zeolite: a highly active and selective catalyst for direct dehydrogenation of propane to propylene. J. Catal. 383, 77–87. https://doi.org/10.1016/j.jcat.2019.12.037.

Dai, Y., Gu, J., Tian, S., et al., 2020. γ-Al_2O_3 sheet-stabilized isolate Co_{2+} for catalytic propane dehydrogenation. J. Catal. 381 482–492. https://doi.org/10.1016/j.jcat.2019.11.026.

Dewangan, N., Ashok, J., Sethia, M., et al., 2019. Cobalt-based catalyst supported on different morphologies of alumina for non-oxidative propane dehydrogenation: effect of metal support interaction and lewis acidic sites. ChemCatChem 11 (19), 4923–4934. https://doi.org/10.1002/cctc.201900924.

Dlamini, M.W., Phaahlamohlaka, T.N., Kumi, D.O., et al., 2020. Post doped nitrogen-decorated hollow carbon spheres as a support for Co Fischer-Tropsch catalysts. Catal. Today 342 99–342110. https://doi.org/10.1016/j.cattod.2019.01.070.

Estes, D.P., Siddiqi, G., Allouche, F., et al., 2016. C-H activation on Co,O sites: isolated surface sites versus molecular analogs. J. Am. Chem. Soc. 138 (45), 14987–14997. https://doi.org/10.1021/jacs.6b08705.

Gao, Y., Han, Z., Hong, S., et al., 2019. ZIF-67-Derived cobalt/nitrogen-doped carbon composites for efficient electrocatalytic N2 reduction. ACS Appl. Energy Mater. 2 (8), 6071–6077. https://doi.org/10.1021/acsaem.9b01135.

Guo, Y., Tang, J., Salunkhe, R.R., et al., 2017. Effect of various carbonization temperatures on ZIF-67 derived nanoporous carbons. Bull. Chem. Soc. Jpn. 90 (8), 939–942. https://doi.org/10.1246/bcsj.20170138.

Han, X., Chen, W.-M., Han, X., et al., 2016. Nitrogen-rich MOF derived porous Co_3O_4/N–C composites with superior performance in lithium-ion batteries. J. Mater. Chem. 4 (34), 13040–13045. https://doi.org/10.1039/c6ta05096d.

Held, A., Kowalska-Kuś, J., Millot, Y., et al., 2018. Influence of the preparation procedure of vanadium-containing SiBEA zeolites on their catalytic activity in propene epoxidation. J. Phys. Chem. C 122 (32), 18570–18582. https://doi.org/10.1021/acs.jpcc.8b05731.

Hu, B., Bean, Getsoian, A., Schweitzer, N.M., et al., 2015. Selective propane dehydrogenation with single-site CoII on SiO2 by a non-redox mechanism. J. Catal. 322, 24–37. https://doi.org/10.1016/j.jcat.2014.10.018.

Hu, Z.-P., Yang, D., Wang, Z., et al., 2019. State-of-the-art catalysts for direct dehydrogenation of propane to propylene. Chin. J. Catal. 40 (9), 1233–1254. https://doi.org/10.1016/s1872-2067(19)63360-7.

Lavrenov, A.V., Saifulina, L.F., Buluchevskii, E.A., et al., 2015. Propylene production technology: today and tomorrow. Catalysis Ind 7 (3), 175–187. https://doi.org/10.1134/s2070050415030083.

Li, X., Wang, P., Wang, H., et al., 2018. Effects of the state of Co species in Co/Al_2O_3 catalysts on the catalytic performance of propane dehydrogenation. Appl. Surf. Sci. 441, 688–693. https://doi.org/10.1016/j.apsusc.2018.02.024.

Lu, J.Z., Yang, L.J., Xu, B.L., et al., 2014. Promotion effects of nitrogen doping into carbon nanotubes on supported iron fischer-tropsch catalysts for lower olefins. ACS Catal. 4 (2), 613–621.

Ma, W., Ackermann, L., 2015. Cobalt(II)-Catalyzed oxidative C–H alkenylations: regio- and site-selective access to isoindolin-1-one. ACS Catal. 5 (5), 2822–2825. https://doi.org/10.1021/acscatal.5b00322.

Motagamwala, A.H., Almallahi, R., Wortman, J., et al., 2021. Stable and selective catalysts for propane dehydrogenation operating at thermodynamic limit. Science 373 (6551), 217–222.

Otroshchenko, T., Radnik, J., Schneider, M., et al., 2016. Bulk binary ZrO_2-based oxides as highly active alternative-type catalysts for non-oxidative isobutane dehydrogenation. Chem. Commun. 52 (52), 8164–8167. https://doi.org/10.1039/c6cc02813f.

Sun, Y-n, Gao, Y-n, Wu, Y., et al., 2015. Effect of sulfate addition on the performance of Co/Al_2O_3 catalysts in catalytic dehydrogenation of propane. Catal. Commun. 60, 42–45. https://doi.org/10.1016/j.catcom.2014.11.024.

Wang, L., Wang, Z., Xie, L., et al., 2019. ZIF-67-Derived N-doped Co/C nanocubes as high-performance anode materials for lithium-ion batteries. ACS Appl. Mater. Interfaces 11 (18), 16619–16628. https://doi.org/10.1021/acsami.9b03365.

Wang, Y., Chen, M., Yang, Z., et al., 2018. Bimetallic Ni-M (M=Co,Cu and Zn)supported on attapulgite as catalysts for hydrogen production from glycerol steam reforming. Appl. Catal. Gen. 550, 214–227. https://doi.org/10.1016/j.apcata.2017.11.014.

Wang, Y., Suo, Y., Ren, J.T., et al., 2021. Spatially isolated cobalt oxide sites derived from MOFs for direct propane dehydrogenation. J. Colloid Interface Sci. 594 113–121. https://doi.org/10.1016/j.jcis.2021.03.023.

Ye, G.H., Wang, H.Z., Duan, X.Z., et al., 2019. Pore network modeling of catalyst deactivation by coking, from single site to particle, during propane dehydrogenation. AIChE J. 65 (1), 140–150.

Yoshizawa, N., Maruyama, K., Yamada, Y., et al., 2000. XRD evaluation of CO_2 activation process of coal-and coconut shell-based carbons. Fuel 79 (12), 1461–1466.

Zhan, T., Liu, X., Lu, S., et al., 2017. Nitrogen doped NiFe layered double hydroxide/reduced graphene oxide mesoporous nanosphere as an effective bifunctional electrocatalyst for oxygen reduction and evolution reactions. Appl. Catal. B Environ. 205 551–558. https://doi.org/10.1016/j.apcatb.2017.01.010.

Zhang, C., Chu, W., Jiang, R., et al., 2019. ZIF-67 derived hollow structured Co_3O_4 nanocatalysts: tunable synthetic strategy induced enhanced catalytic performance. Catal. Lett. 149 (11), 3058–3065. https://doi.org/10.1007/s10562-019-02871-y.

Zhang, H., Ma, Z., Duan, J., et al., 2015. Active sites implanted carbon cages in core–shell architecture: highly active and durable electrocatalyst for hydrogen evolution reaction. ACS Nano 10 (1), 684–694. https://doi.org/10.1021/acsnano.5b05728.

Zhang, L., Su, Z., Jiang, F., et al., 2014. Highly graphitized nitrogen-doped porous carbon nanopolyhedra derived from ZIF-8 nanocrystals as efficient

electrocatalysts for oxygen reduction reactions. Nanoscale 6 (12), 6590–6602. https://doi.org/10.1039/c4nr00348a.
Zhao, D., Li, Y., Han, S., et al., 2019a. ZnO nanoparticles encapsulated in nitrogen-doped carbon material and silicalite-1 composites for efficient propane dehydrogenation. iScience 13, 269–276. https://doi.org/10.1016/j.isci.2019.02.018.
Zhao, D., Li, Y.M., Han, S.L., et al., 2019b. ZnO nanoparticles encapsulated in nitrogen-doped carbon material and silicalite-1 composites for efficient propane dehydrogenation. iScience 13, 269–276.
Zhao, Y., Sohn, H., Hu, B., et al., 2018. Zirconium modification promotes catalytic activity of a single-site cobalt heterogeneous catalyst for propane dehydrogenation. ACS Omega 3 (9), 11117–11127. https://doi.org/10.1021/acsomega.8b00862.